



Controlled Synthesis of Hollow α -Fe₂O₃ Microspheres Assembled With Ionic Liquid for Enhanced Visible-Light Photocatalytic Activity

Hang Yin^{1†}, YuLing Zhao^{1†}, Qingsong Hua², Jianmin Zhang², Yuansai Zhang¹, Xijin Xu³, Yunze Long¹, Jie Tang^{4*} and Fengyun Wang^{1,5*}

¹ College of Physics and State Key Laboratory of Bio-Fibers and Eco-Textiles, Qingdao, China, ² National Engineering Research Center for Intelligent Electrical Vehicle Power System, Power & Energy Storage System Research Center, Qingdao University, Qingdao, China, ³ School of Physics and Technology, University of Jinan, Jinan, China, ⁴ 1D Nanomaterials Group, National Institute for Materials Science, Tsukuba, Japan, ⁵ Key Laboratory of Microelectronic Devices & Integrated Technology, Institute of Microelectronics, Chinese Academy of Sciences, Beijing, China

OPEN ACCESS

Edited by:

Tianyi Ma,
University of Newcastle, Australia

Reviewed by:

Aihua Xu,
Wuhan Textile University, China
Gang Zhao,
University of Jinan, China
Huan Pang,
Yangzhou University, China

*Correspondence:

Jie Tang
tang.jie@nims.go.jp
Fengyun Wang
fywang777@163.com

[†]These authors have contributed
equally to this work

Specialty section:

This article was submitted to
Catalysis and Photocatalysis,
a section of the journal
Frontiers in Chemistry

Received: 08 November 2018

Accepted: 21 January 2019

Published: 27 February 2019

Citation:

Yin H, Zhao Y, Hua Q, Zhang J,
Zhang Y, Xu X, Long Y, Tang J and
Wang F (2019) Controlled Synthesis of
Hollow α -Fe₂O₃ Microspheres
Assembled With Ionic Liquid for
Enhanced Visible-Light Photocatalytic
Activity. *Front. Chem.* 7:58.
doi: 10.3389/fchem.2019.00058

Porous self-assembled α -Fe₂O₃ hollow microspheres were fabricated via an ionic liquid-assisted solvothermal reaction and sequential calcinations. The concentration of the ionic liquid (1-butyl-3-methylimidazolium tetrafluoroborate [C₄Mim]BF₄) was found to play a crucial role in the control of these α -Fe₂O₃ hollow structures. Trace amounts ionic liquid was used as the soft template to synthesize α -Fe₂O₃ hollow spheres with a large specific surface (up to 220 m²/g). Based on time-dependent experiments, the proposed formation mechanisms were presented. Under UV light irradiation, the as-synthesized α -Fe₂O₃ hollow spheres exhibited excellent photocatalysis in Rhodamine B (RhB) photodegradation and the rate constant was 2–3 times higher than α -Fe₂O₃ particles. The magnetic properties of α -Fe₂O₃ hollow structures were found to be closely associated with the shape anisotropy.

Keywords: α -Fe₂O₃, assembly, porous materials, ionic liquid, magnetic properties, visible light, photocatalytic activity

INTRODUCTION

Nanostructured oxides with a variety of useful functionalities are widely applied in photocatalysis, energy storage, etc. (Guo et al., 2017; Li et al., 2017; Zhao et al., 2017, 2018). In particular, hematite (α -Fe₂O₃), an environmentally-friendly magnetic photocatalyst ($E_g = 2.2$ eV), has been identified as an important material because of its potential for a wide range of practical applications (Brezesinski et al., 2011; Yang et al., 2014; Zhou et al., 2014; Ma et al., 2018). Recently, self-assembled hematite with highly specific hollow nano/micro-structures and unique properties has emerged as being of great interest to material scientists. To date, various self-assembled hollow α -Fe₂O₃ nano/micro-structures have been prepared by different synthetic techniques, including the two-step reaction process (Yu J. et al., 2009), hydrothermal (Xu et al., 2012), and solvothermal approaches (Song et al., 2012; Zhu et al., 2012), thermal oxidation at high temperature (Xie et al., 2010), etc. For example, Yu and co-workers successfully fabricated cage-like Fe₂O₃ hollow spheres and carbonaceous polysaccharide spheres were used as porous crystalline shell templates, followed by calcination at 500°C for 4 h. Song and co-workers proposed a hydrolysis route to synthesis Fe₂O₃ hierarchical hollow spheres, via a sodium dodecyl benzenesulfonate (SDBS)-assisted hydrolysis

process. However, these template methods often suffer from a problem: it is difficult to remove the template and surface-active agent completely. Furthermore, template removal always leads to additional problems in sample morphology. Therefore, it is still necessary to develop a simple route to synthesizing assembled hollow α -Fe₂O₃ structures.

Ionic liquids (ILs), or “designer liquids,” are known for their superior properties such as recyclability and stable chemical properties. They are used extensively in catalysis, separations, electrochemistry, and especially nanochemistry (Welton, 1999; Wasserscheid and Keim, 2000; Seddon, 2003). The most important advantage of ILs is that they can form extended hydrogen bond systems in the liquid, thereby enabling highly-structured nanostructures (Mele et al., 2003). This special performance can be used as the “entropic driver” for synthesis of self-assembled nanostructures. It has been proved that ILs can be used not only as solvents, but also as templates for preparing nanomaterials with improved properties (Endres et al., 2003; Cooper et al., 2004; Liu et al., 2006). For instance, a variety of nano/micro-structures have been synthesized via ILs, especially assembled hollow structures such as Bi₄O₅Br₂ and BiOBr spheres (Xia et al., 2011a; Mao et al., 2017) and α -Fe₂O₃ hollow polyhedral (Xu et al., 2013). These hollow structures may also exhibit unique properties for photocatalysis.

In this work, we report a simple and feasible ionic liquid-assisted solvothermal method to synthesize self-assembled α -Fe₂O₃ hollow microspheres. The ionic liquid [C₄Mim]BF₄ acts as a soft template can be easily removed by annealing in air. Compared with α -Fe₂O₃ particles, the as-synthesized α -Fe₂O₃ hollow spheres exhibit enhanced photocatalytic activity due to their porous self-assembly structure and higher surface area. As far as we know, α -Fe₂O₃ porous hollow microspheres with high surface area (above 200 m²/g) prepared via this ionic liquid-assisted solvothermal synthesis route is reported for the first time. Additionally, the possible formation mechanisms have also been proved. The as-prepared α -Fe₂O₃ samples exhibit ferromagnetic properties and can be recycled easily.

EXPERIMENTAL

Materials and Methods

Materials

Ferric chloride (FeCl₃·6H₂O, 99%) and ethylenediamine (EDA) were purchased from Tianjin Damao Chemical Co. The ionic liquid ([C₄mim]BF₄) was obtained from Beijing Solarbio Technology Co. Ethylene glycol (EG) was purchased from Tianjin Chemical Reagent Co. and distilled water was used throughout the experiment.

Synthesis

In a typical experimental process, FeCl₃·6H₂O (0.81 g) was dissolved into 60.0 mL of ethylene glycol (EG). Then, 0, 0.1, 0.2, 0.3, 0.4, and 0.5 mL of [C₄Mim]BF₄ were added to the above solution. After 2 h, 3 mL of ethylenediamine (EDA) was added into the mixture solution to form a well-distributed emulsion. After 1 h, the emulsion was transferred into a Teflon-sealed autoclave with a capacity of 100 mL, sealed and heated at

200°C for 20 h. After cooling to room temperature, the resultant precipitate was washed with deionized water and ethanol several times until the solution was neutral. After drying in a vacuum oven at 60°C for 6 h, the dried products were calcined in air at 250°C for 6 h. The reaction time was adjusted to study the mechanism.

Materials Characterization

X-ray diffraction (XRD) patterns were obtained with a Rigaku RINT 2500 diffractometer using a Cu-K α radiation source ($\lambda = 1.5406$ Å). The morphology and microstructure of the as-prepared samples were examined with scanning electron microscopy (SEM, JEOL 6500F). TEM and HRTEM images were recorded with a Tecnai accelerating voltage of 120 and 200 kV, respectively. The nitrogen adsorption/desorption isotherms at 77.35 K were collected on an AUTOSORB iQ-MP instrument after heating the samples at 150°C for 2 h. The surface areas were estimated using the Brunauer-Emmett-Teller (BET) method in the relative pressure range of 0.05–0.3. Pore size distributions were analyzed using nitrogen adsorption data in a Barrett-Joyner-Halenda (BJH) model. Magnetic properties of the as-synthesized samples were measured with a physical property measurement system (PPMS-9T, ever cool II, USA).

Photocatalytic Reaction

20.0 mg of α -Fe₂O₃ photocatalyst catalyst and 50.0 mL of RhB dye aqueous solution (10.0 mg/L) were mixed in a Pyrex reactor and stirred in the dark for 30 min to reach a complete absorption/desorption equilibrium. Afterwards, the suspension was exposed to a 300 W Xenon lamp and stirred simultaneously. Subsequently, 3.0 mL of suspension was centrifuged at 5,000 rpm for 4 min to remove the photocatalyst. Finally, the concentration of RHB was monitored with a TU-1901 UV-vis spectrophotometer by monitoring the absorbance at 553 nm.

RESULTS AND DISCUSSION

Structure and Morphology Characterization

The purity and crystallinity of the as-prepared powder samples are measured by XRD (Figure 1). The XRD shows that all diffraction peaks can be indexed in α -Fe₂O₃ (JCPDS 33-0664) with structural parameters of $a = b = 5.038$ Å, $c = 13.749$ Å, $\alpha = \beta = 90^\circ$, and $\gamma = 120^\circ$. No other peaks are observed, demonstrating that the α -Fe₂O₃ products have high-purity and a single phase. Therefore, we can infer that anions and cations of the [C₄Mim]BF₄ are not doped into the α -Fe₂O₃ lattice. As the [C₄Mim]BF₄ addition increases, the peak intensities of α -Fe₂O₃ also gradually increase, indicating that sample (D) has the highest degree of crystallization. This result proves that the addition of ionic liquid can enhance the crystallization of as-synthesized materials. A similar phenomenon is also observed in the previous report (Xu et al., 2013).

According to the full width at half-maximum (fwhm) of the diffraction peaks, the average crystallite size of the α -Fe₂O₃ nanoparticles and microspheres ([C₄Mim]BF₄ = 0.1, 0.2,

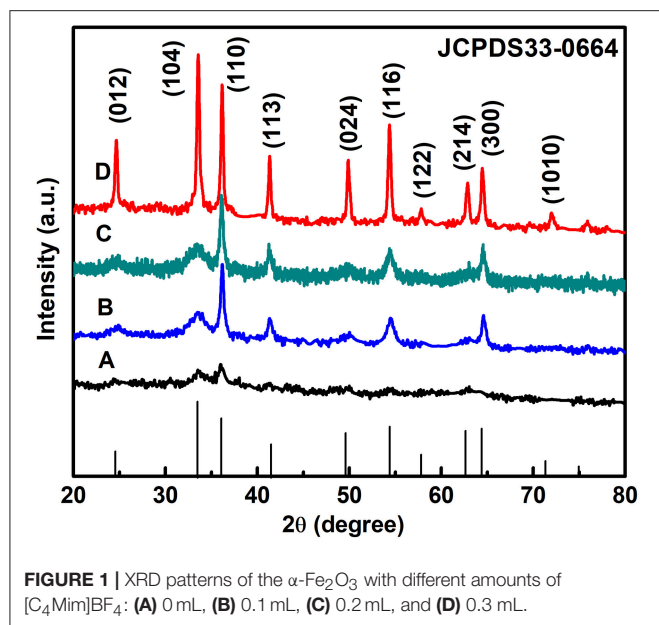


FIGURE 1 | XRD patterns of the α -Fe₂O₃ with different amounts of [C₄Mim]BF₄: (A) 0 mL, (B) 0.1 mL, (C) 0.2 mL, and (D) 0.3 mL.

0.3 mL) can be estimated from the Scherrer equation to be about 40.2, 84.6, 101.2, and 198.5 nm, respectively.

$$D_{hkl} = K\lambda / (\beta_{hkl} \cos \theta_{hkl})$$

where D_{hkl} is the particle size perpendicular to the normal line of (hkl) plane, K is a constant (it is 0.9), β_{hkl} is the full width at half-maximum of the (hkl) diffraction peak, θ_{hkl} is the Bragg angle of (hkl) peak, and λ is the wavelength of X-ray.

The morphology and structure of the as-prepared samples are studied by SEM and TEM **Figure 2** shows the typical SEM micrographs of the α -Fe₂O₃ samples prepared with varying [C₄Mim]BF₄ additions at 200°C for 20 h. In the absence of [C₄Mim]BF₄ (**Figures 2A–C**), only α -Fe₂O₃ pseudo cubic particles are formed. The morphology and size of α -Fe₂O₃ particles are non-uniform and the alignment is disordered. As the amount of [C₄Mim]BF₄ increased from 0.1 to 0.3 mL, the as-prepared α -Fe₂O₃ changed from irregular particles to the uniform microspheres.

Figures 2D–F show the SEM image of [C₄Mim]BF₄ = 0.1 mL, which is composed of nanoparticles. When the addition of [C₄Mim]BF₄ is up to 0.2 mL, perfectly spherical α -Fe₂O₃ is formed. As shown in **Figure 2G**, some broken α -Fe₂O₃ microspheres reveal that the as-obtained α -Fe₂O₃ microspheres are of a hollow structure. Therefore, we can infer that [C₄Mim]BF₄ is used as a template in the process of α -Fe₂O₃ synthesis. The three-tiered organization of crystallites for these hollow dandelions is shown in the magnified image (**Figure 2H**). Numerous nanosheets are present on the surface of the dandelion spheres, with a puffy appearance and the average diameter being about 6.5 μ m. From **Figure 2I**, we can see that individual nanosheets have an average size of about 100 nm, which is in agreement with the result calculated from Scherrer's formula. When the [C₄Mim]BF₄ amount increases to

0.3 mL (**Figures 2J,H,L**), the similar nanosheets stack up in three-dimensional ordered microspheres (5.0–7.0 μ m) with a larger thickness (about 200 nm). **Figure 3A** shows the TEM image of an α -Fe₂O₃ microsphere. However, the structure in [C₄Mim]BF₄ = 0.3 mL demonstrates no internal void space. A high-resolution TEM (HRTEM) image (**Figure 3B**) exhibited lattice spacing of 0.252 nm, corresponding to the (110) lattice plane. Additionally, some examples of synthesizing nanostructured α -Fe₂O₃ using different kinds of ILs are given in **Table 1**.

Additionally, the self-assembly micron spheres are made up of a bunch of nanosheets, indicating that the spheres are porous in structure. It is striking that when the addition of [C₄Mim]BF₄ reaches to 0.4 mL, precipitation is very sparse. Until 0.5 mL, no precipitation synthesized after reaction. This phenomenon can be explained as follows: EG and ionic liquids are not mutually soluble, so the two-phase interface is formed. With an increase in the addition of ionic liquids, the disorder of atoms at the two-phase interface increases, resulting in a growing of interfacial energy, which lifts the nucleation resistance. Owing to large resistance, crystal cannot nucleate.

Nitrogen Sorption

Figure 4 shows the nitrogen adsorption-desorption isotherms and pore size distributions of the as-prepared α -Fe₂O₃. The isotherms of α -Fe₂O₃ samples shown in **Figure 4A** are of type IV with a hysteresis loop from 0.5 to 1.0 (P/P₀). The BET-specific surface areas of α -Fe₂O₃ hollow microspheres are calculated to be 183, 208, and 221 m²g⁻¹, all larger than that of α -Fe₂O₃ synthesized without [C₄Mim]BF₄ (only 44 m²g⁻¹). Correspondingly, the BJH pore size of the as-synthesized α -Fe₂O₃ ranges from 5.0 to 10.0 nm (**Figure 4B**). The smaller pore structures may arise from the crystal growth, and the larger pores ascribe to the stacking of the α -Fe₂O₃ nano-structures and the hollow structure. Additionally, the peaks of the pore sizes of the α -Fe₂O₃ move to the right after adding [C₄Mim]BF₄, showing that average pore size increases. From this result, we can infer that the crystallinity of the as-prepared α -Fe₂O₃ improved (Zhu et al., 2012), which is in agreement with the XRD analysis. **Table 2** summarizes the mean pore size and S_{BET} of the as-obtained α -Fe₂O₃. It shows that with increasing additions of [C₄Mim]BF₄, S_{BET} increases dramatically. This result may be attributed to two factors: first, compared with irregular α -Fe₂O₃ nanoparticles or nanosheets, hollow assembly structures have more opportunities to participate in nitrogen adsorption. Without the [C₄Mim]BF₄, the specific surface area of α -Fe₂O₃ is only 44.0 m²g⁻¹ (Xia et al., 2011b). Second, the presence of a large number of mesoporous structures (6–7 nm) leads to a large specific surface area.

Possible Formation Mechanism of α -Fe₂O₃ Hollow Spheres

To better understand the formation process of the α -Fe₂O₃ porous hollow spheres, time-dependent experiments were carried out. As shown in **Figures 5A–D**, representative SEM images at different time intervals are displayed. First, a hollow core-shell spherical structure was generated at 10 h. The mean diameter of the core is about 2.0 μ m, which was further confirmed by the TEM image shown in **Figure S1**. Second, some

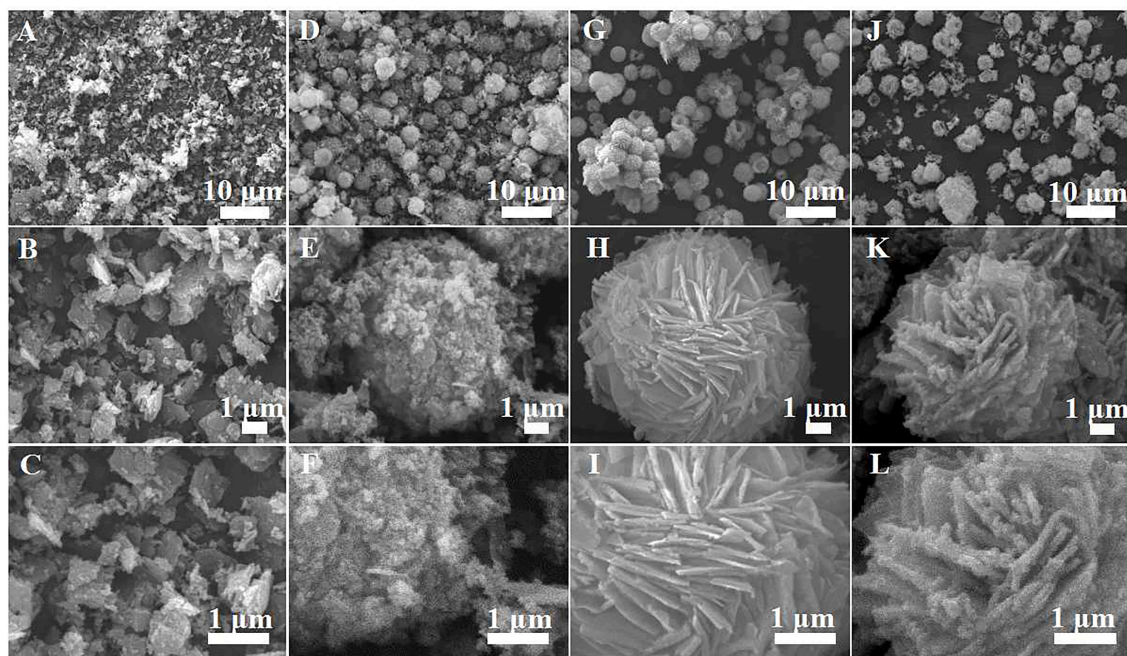


FIGURE 2 | SEM images of α -Fe₂O₃ samples prepared with varying addition of [C₄Mim]BF₄ at 200°C for 20 h: (A–C) 0 mL, (D–F) 0.1 mL, (G–I) 0.2 mL, (J–L) 0.3 mL.

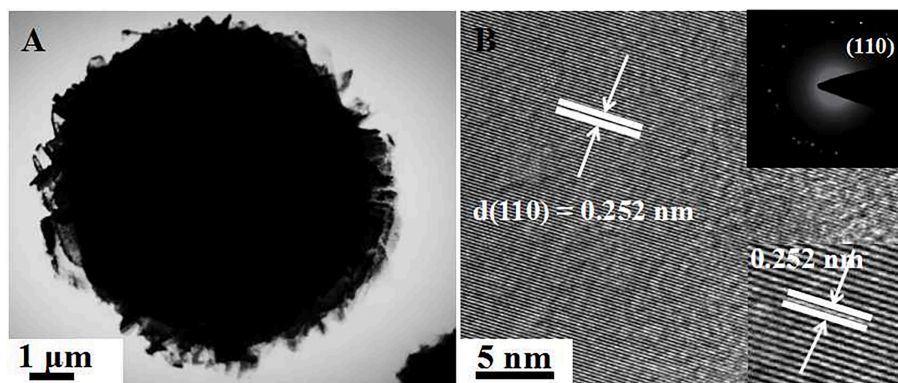


FIGURE 3 | (A) TEM image of single sphere obtained at [C₄Mim]BF₄ = 0.3 mL, (B) HRTEM image. The inset shows the corresponding SAED pattern (up-right).

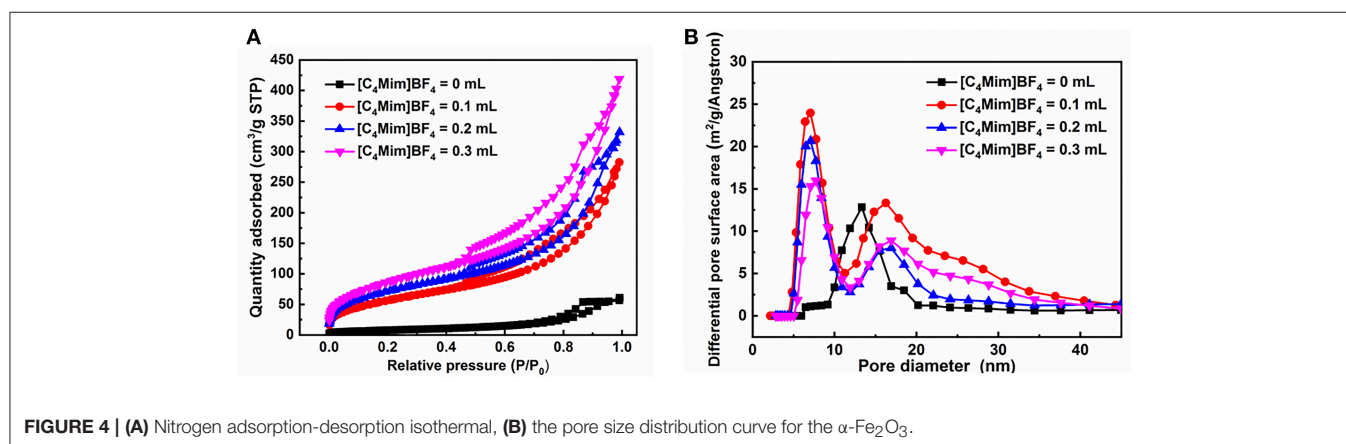
microparticles were deposited on its surface at 14 h. Then, as the reaction time reached 16 h, some nanosheets began to cover the surface of the nuclei, indicating that deposition was still in progress. When the duration reached 20 h, a hollow sphere covered with a great number of nanosheets was obtained.

Based on the above experimental results, the nucleation and growth mechanism for the microsphere in the two-phase system was proposed, as shown in **Figure 6**. First, Fe³⁺ reacted with EDA in EG-[C₄Mim]BF₄ solution to form a relatively stable complex ion of [Fe(EDA)³]³⁺ (Zhang et al., 2006). High temperature caused complex ions [Fe(EDA)³]³⁺ to decompose into FeOOH. Thus, FeOOH was first formed. Then, the FeOOH nanoparticles dissolved and reacted with the obtained Fe²⁺ in a [C₄Mim]BF₄

assisted system to form α -Fe₂O₃ nanoparticles. From **Figure 5E**, the peaks of FeOOH and α -Fe₂O₃ can be observed at 10 h. The formed α -Fe₂O₃ nanoparticles were unstable and had a tendency to form larger congeries, which may have been driven by the minimization of interfacial energy. That is why after 14 h, the sample only showed the crystal image of α -Fe₂O₃. However, EG solution has greater viscosity and fewer surface hydroxyls than the aqueous solution, resulting in kinetically slower nucleation and aggregation of nanocrystals, which lead to the formation of perfectly oriented assemblies by the adequate rotation to find the low-energy configuration interface (Zhu et al., 2013). A longer reaction time leads to directional alignment to generate spherical nuclei at 10 h. During the subsequent

TABLE 1 | Comparison of different α -Fe₂O₃ samples synthase by this work and others reported in previous references.

Reaction system	Ionic liquid	Morphology	Size	References
Ethanol + NaOH	[OmMim]FeCl ₄	Microspheres	2–4 μ m	Xu et al., 2013
water + NaOH	[BMim]Cl	Microcubes	600 nm	Lian et al., 2009
Water + CH ₃ COOK	[BMim]Cl	Mesoporous hollow Microspheres	1 μ m	Lian et al., 2009
Urea + water	[C ₄ Mim]BF ₄	Hollow polyhedral	0.5–1 μ m	Xu et al., 2012
Urea + [C ₁₂ Mim] Br	[C ₁₂ Mim] Br	Nanorods	Diameter 30 nm Length 200 nm	Ping et al., 2017
EG + NaOH	[C ₂ Mim] [C ₂ OSO ₃]	Nanoparticles	12–47 nm	Shikha et al., 2015
EG + EDA	[C ₄ Mim]BF ₄	Microspheres	5–7 μ m	This work

**FIGURE 4** | (A) Nitrogen adsorption-desorption isothermal, (B) the pore size distribution curve for the α -Fe₂O₃.**TABLE 2** | Brumaire–Emmett–Teller (BET) surface area and mean pore diameters of the as-prepared samples.

Sample	Addition (mL)	BET surface areas (m ² g ⁻¹)	BJH pore size (nm)
1	0	44	13.33
2	0.1	183	6.42
3	0.2	208	7.08
4	0.3	221	7.71

process, nanoparticles gradually assemble into nanosheets and stack on the surface of the template. The reason for the formation of nanosheets is that small particles gradually adhere to large particles to form thin sheets, which is commonly referred as Ostwald ripening. Finally, a specified morphology forms. Such a process is also observed in several other reports (Lou et al., 2006; Zhu et al., 2008; Yu X. et al., 2009). In this study, the adjacent primary ferric alkoxide nanocrystals have high activity due to their high surface energy. They further grow into nanosheets by directional aggregation, which greatly reduces the interface energy of small primary nanocrystals. Then, by directional attachment and self-assembly, the nanosheets gradually evolve into 3D flower-like superstructures. At the same time, it is combined with the mature process of Ostwald to form a favorable hollow structure.

In this formation process, the reaction time is one of the most important controlling factors. Apart from the reaction time,

EDA is also a critical factor. EDA is used as a precipitant during this process. When a part of an EG molecule loses protons and coordinates with FeCl₃ to form ferric alkoxide, H⁺ is produced in the reaction of EG with metal chloride. If H⁺ cannot be removed, the accumulation of H⁺ will inhibit the formation of further iron oxides. In this paper, EDA takes the lead to react with Fe³⁺ to form a stable complex and inhibit the formation of H⁺ in the reaction system.

Enhancement of Photocatalytic Activity

The photocatalytic degradation of RhB is monitored by measuring the absorption behavior of the solution at 553 nm. The evolutions of the spectrums are shown in **Figure 7A** for α -Fe₂O₃ synthesized without [C₄Mim]BF₄ and in **Figure 7B** for that synthesized with 0.3 mL [C₄Mim]BF₄. When the addition amount reaches 0.3 mL, 90% of RhB is decomposed after 90 min irradiation, while it is no more than 50% for the sample synthesized without [C₄Mim]BF₄. Thus, the use of [C₄Mim]BF₄ in the synthesis process effectively improves the photocatalytic performance. To clarify the effect of [C₄mim]BF₄, we figure out the rate constants of the degradation processes for the α -Fe₂O₃ synthesized with various concentrations of [C₄Mim]BF₄. To evaluate the reactivity, the apparent reaction rate constant (*k*) is calculated. **Figure 7C** shows ln(C/C₀)–t plots for the α -Fe₂O₃ samples synthesized with different [C₄Mim]BF₄ amounts as well as the blank test. The rate constant *k* is 0.00756, 0.00927, 0.0183, 0.0212 min⁻¹ for [C₄Mim]BF₄ = 0.0, 0.1, 0.2, and 0.3 mL,

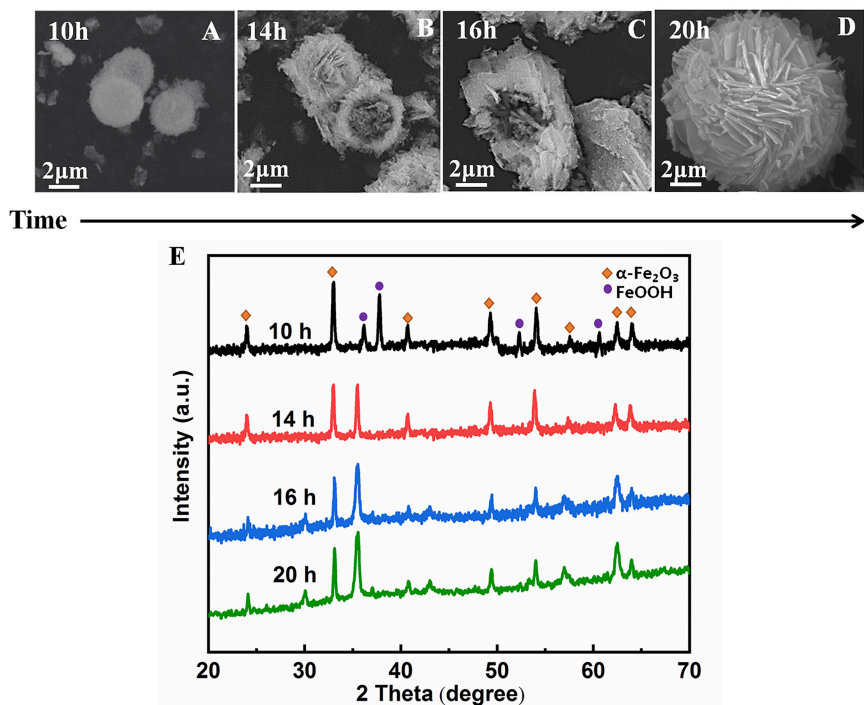


FIGURE 5 | SEM images of α -Fe₂O₃ hollow microsphere structures synthesized in the presence of ionic liquid [C₄Mim]BF₄ = 0.2 mL at 200°C. (A) 10 h, (B) 14 h, (C) 16 h, (D) 20 h. (E) XRD patterns of the α -Fe₂O₃ at different time.

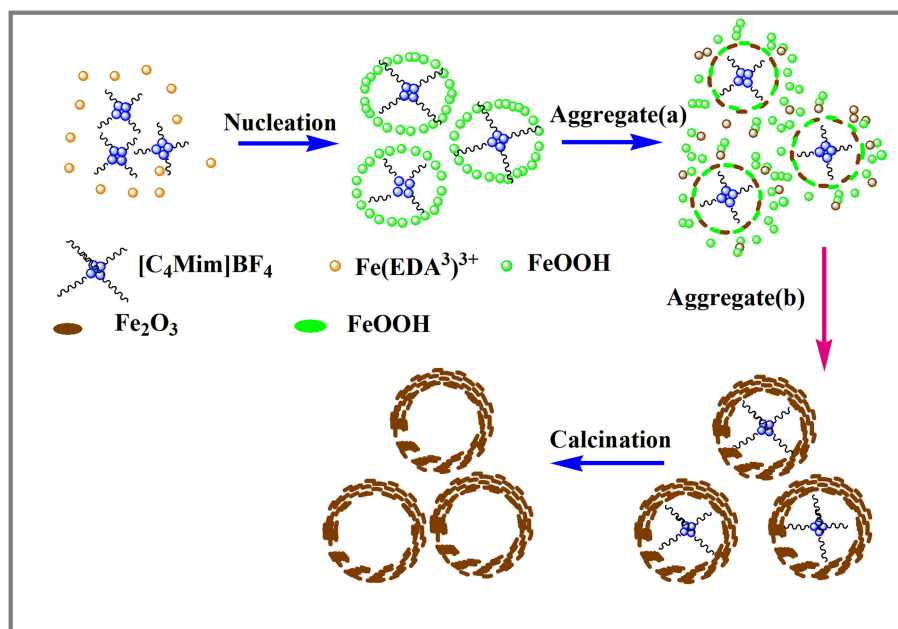


FIGURE 6 | Schematic illustration of the formation of α -Fe₂O₃ hollow spheres.

respectively, shown in **Figure 7D**. Thus, the photocatalytic performance is found to improve with increasing [C₄Mim]BF₄ addition amounts. As shown in **Figure 7E**, we carried out a coarse comparison of degradation efficiencies between this

study and other studies based on the photodegradation of RhB by α -Fe₂O₃.

In addition to the high catalytic efficiency, the catalyst possessed robust stability. In our case, α -Fe₂O₃ samples with the

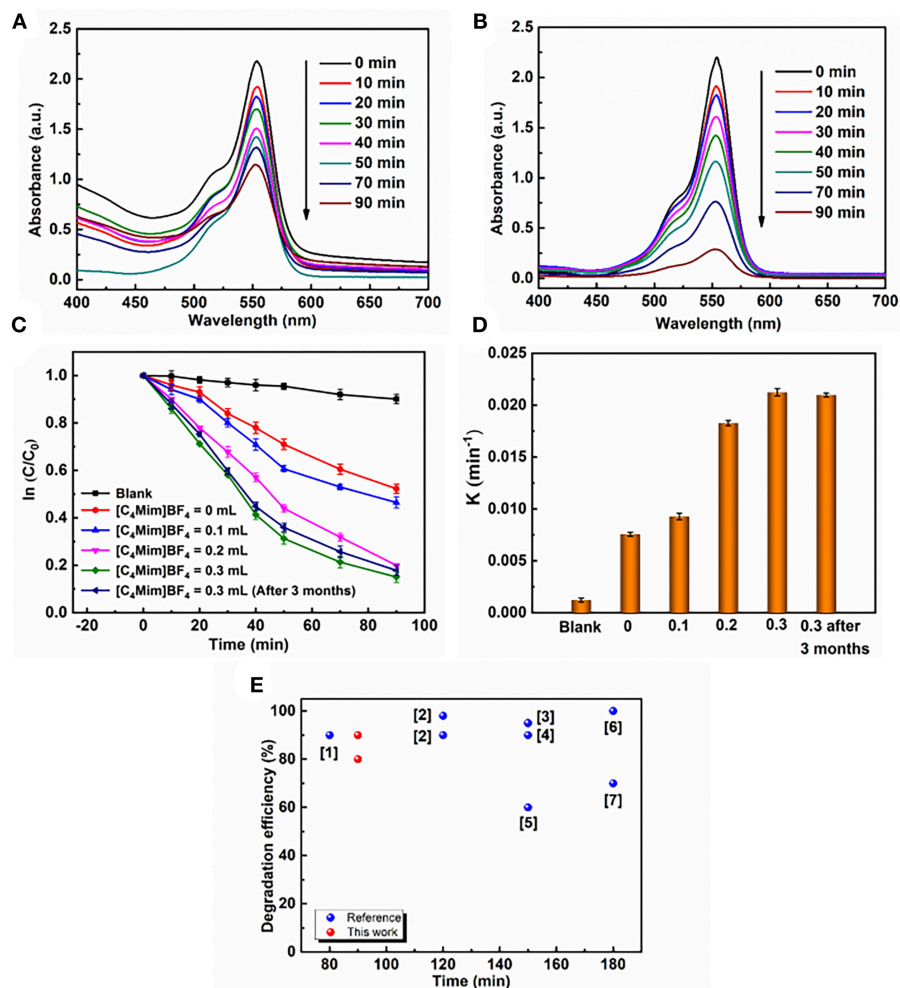


FIGURE 7 | UV-vis absorption spectra during photocatalytic reaction of RhB over α -Fe₂O₃ with different [C₄Mim]BF₄ additions at different time intervals: **(A)** 0 mL, **(B)** 0.3 mL, **(C)** plots of $\ln(C/C_0)$ against time t of various samples: without catalyst, the α -Fe₂O₃ hollow spheres prepared with addition = 0, 0.1, 0.2, and 0.3 mL, respectively. **(D)** Reaction kinetics of RhB degradation under visible light irradiation by α -Fe₂O₃. **(E)** Comparison of degradation efficiencies of different α -Fe₂O₃ samples during the RhB photodegradation driven by visible light. Red balls refer to the α -Fe₂O₃ samples prepared in this work and blue balls refer to the α -Fe₂O₃ samples reported in previous references. ([1] Xu et al., 2012; [2] Pawar and Choi, 2015); [3] (Cai et al., 2014); [4] (Xu et al., 2012); [5] (Liang et al., 2014); [6] (Zhou et al., 2011); [7] (Wu et al., 2013)).

amount of 0.3 mL [C₄Mim]BF₄ also have stable photoactivity. After 3 months, the degradation rate of RhB has little change in k value (**Figure 7D**). An SEM image of the sample after placement for 3 months is shown in **Figure S2**. It shows that the morphology and structure of the as-synthesized α -Fe₂O₃ have few changes, which is very important for maintaining the photocatalytic activity of samples.

The photocatalytic activities of the α -Fe₂O₃ are closely related to its energy band. **Figure 8A** shows UV-vis diffuse reflectance spectra of α -Fe₂O₃ with additions of [C₄Mim]BF₄ = 0 and 0.3 mL in the wavelengths of 200–800 nm. Although the α -Fe₂O₃ particles and spheres show similar optical properties, the microsphere with a [C₄Mim]BF₄ addition of 0.3 mL shows stronger absorption, from 600 to 800 nm, resulting in a larger surface area that can absorb more light (Wang et al., 2011).

Therefore, the as-prepared α -Fe₂O₃ microspheres exhibit better photocatalytic performance. **Figure 8B** is the plot of $(\alpha h\nu)^2$ vs. the energy of the absorbed light for α -Fe₂O₃. From **Figure 8B**, the band gap is determined to be 2.05 eV for the α -Fe₂O₃, indicating that the oxygen vacancies do not change the band gaps of α -Fe₂O₃ microstructures significantly.

Furthermore, in the process of photocatalytic reaction, \cdot OH is considered to be another main reaction species leading to the oxidative decomposition of organic pollutants. However, it was revealed that \cdot OH could not be generated during irradiation for Fe₂O₃ (Xiang et al., 2011). Because the photo-generated holes and electrons on Fe₂O₃ could not react with OH⁻/H₂O and O₂ to form \cdot OH and O₂²⁻, respectively, no \cdot OH can be generated in Fe₂O₃ (Xiang et al., 2011). This indicates that reactive species other than \cdot OH are present. However,

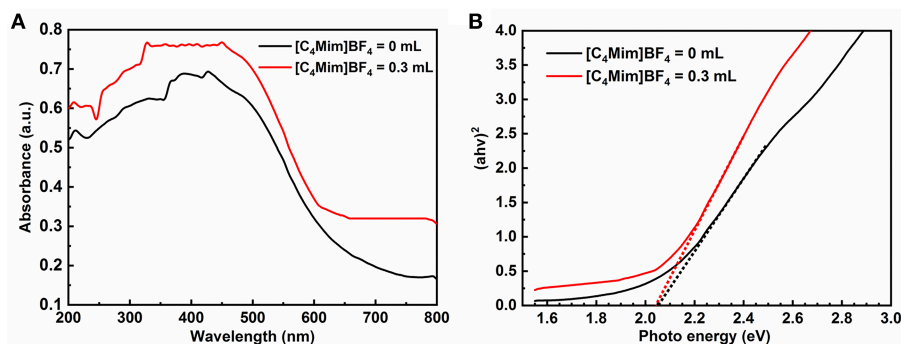


FIGURE 8 | (A) UV-vis diffuse reflectance spectra and **(B)** plots of $(\alpha hv)^2$ vs. photon energy $h\nu$ of the samples with addition = 0, 0.3 mL.

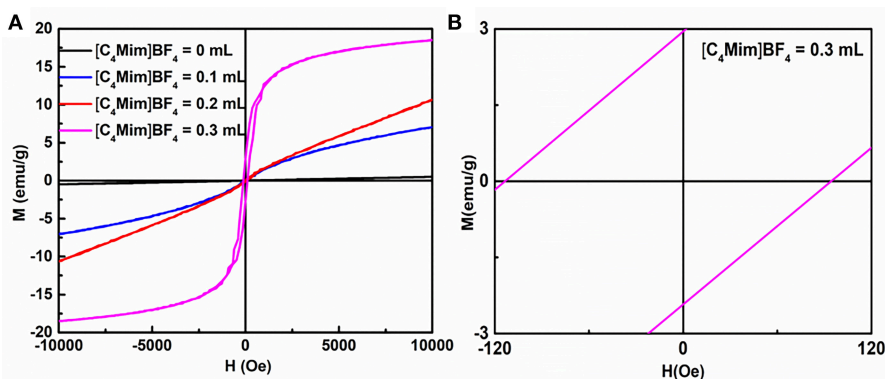


FIGURE 9 | (A) Magnetization loops for α -Fe₂O₃ particles synthesized with different additions of [C₄Mim]BF₄. **(B)** A magnified view of curve.

several research results suggest that photo-generated holes and electrons can directly give rise to photocatalytic oxidation. As shown in this study, the photocatalytic performances of these α -Fe₂O₃ samples strongly depend on the [C₄Mim]BF₄ concentrations in the synthesis process. Therefore, it is likely that the high photocatalytic activity results from the novel structure, large surface area and strong absorption of visible light. Generally, large specific surface area provides more unsaturated coordination, which helps to improve the efficiency of electron hole separation (Tang et al., 2004). Furthermore, the increase of unsaturated coordination sites may improve the surface electron transfer rate. The increase of the surface electron transfer rate leads to the reduction of the probability of recombination and, therefore, the photo-generated charge carriers could more easily transfer to the surface to degrade the adsorbed RhB.

Magnetic Properties

It is well-known that α -Fe₂O₃ exhibits ferromagnetism (Sun et al., 2010). **Figure 9** and **Figure S3** shows the room temperature magnetic hysteresis loops and the magnetic field sweeping from -10.0 to 10.0 k Oe. **Table 3** collects the values of remnant magnetization (M_r) and coercivity (H_c) of the as-synthesized α -Fe₂O₃ samples. It can be determined from the shape of

TABLE 3 | The values of remnant magnetization (M_r) and coercivity (H_c) of the as-synthesized samples.

Samples	0 mL	0.1 mL	0.2 mL	0.3 mL
M_r (emu/g)	0.003	0.095	0.15	2.99
H_c (Oe)	32.72	41.99	51.97	100.44

the hysteresis loop that the synthesized α -Fe₂O₃ sample shows ferromagnetism. Additionally, the hysteresis loop did not reach saturation up to the maximum applied magnetic field, because of the presence of large-shape anisotropy (Bharathi et al., 2010). It is also shown in **Table 3** that the residual magnetization and coercivity of assembled microspheres of α -Fe₂O₃ are large than α -Fe₂O₃ nanoparticles. It is widely understood that the morphology and structure of the as-synthesized samples will greatly affect the magnetization of ferromagnetic materials (Sorescu et al., 1999). Therefore, the assembly of the nano-sized and oriented particles and sheets into non-random structure results in the change of the single domain to the multidomain, leading to higher remnant magnetization and coercivity (Park et al., 2000). In summary, the difference can be attributed to the high crystallization, single domain size, surface (Tong et al., 2015), structure, and shape.

CONCLUSION

In summary, porous self-assembled α -Fe₂O₃ hollow microspheres were successfully prepared via a facile ionic liquid assistant synthesis approach. A nucleation–aggregation evacuation mechanism was the main formation of the porous hollow structures. EDA and [C₄Mim]BF₄ play significant roles on the formation of porous α -Fe₂O₃ hollow spheres. The increase in [C₄Mim]BF₄ promotes photocatalytic activities and α -Fe₂O₃ microspheres show higher photocatalytic activities. We believe that high specific surface area and porous hollow structure play an important role in improving the photocatalytic performance of as-prepared α -Fe₂O₃. Additionally, when the addition amount reaches 0.3 mL, the synthesized samples show ferromagnetism and can be easily recycled. The α -Fe₂O₃ hollow porous spheres prepared by our method have high photocatalytic activity, ideal ferromagnetic properties, and high specific surface area. They are expected to exhibit use as applications in sensors, catalysis, separation technology, environmental engineering, controlled drug delivery, and more.

DATA AVAILABILITY

All datasets generated for this study are included in the manuscript and/or the **Supplementary Files**.

REFERENCES

- Bharathi, S., Nataraj, D., Seetha, M., Mangalaraj, D., Ponpandian, N., Masuda, Y., et al. (2010). Controlled growth of single-crystalline, nanostructured dendrites and snowflakes of α -Fe₂O₃: influence of the surfactant on the morphology and investigation of morphology dependent magnetic properties. *CrystEngComm* 12, 373–382. doi: 10.1039/B910550F
- Brezesinski, K., Haetge, J., Wang, J., Mascotto, S., Reitz, C., Rein, A., et al. (2011). Ordered mesoporous α -Fe₂O₃ (hematite) thin-film electrodes for application in high rate rechargeable lithium batteries. *Small* 7, 407–414. doi: 10.1002/smll.201001333
- Cai, J., Chen, S., Ji, M., Hu, J., Ma, Y., and Qi, L. (2014). Organic additive-free synthesis of mesocrystalline hematite nanoplates via two-dimensional oriented attachment. *CrystEngComm* 16, 1553–1559. doi: 10.1039/C3CE41716F
- Cooper, E. R., Andrews, C. D., Wheatley, P. S., Webb, P. B., Wormald, P., and Morris, R. E. (2004). Ionic liquids and eutectic mixtures as solvent and template in synthesis of zeolite analogues. *Nature* 430:1012. doi: 10.1038/nature02860
- Endres, F., Bukowski, M., Hempelmann, R., and Natter, H. (2003). Electrodeposition of nanocrystalline metals and alloys from ionic liquids. *Angew. Chem. Int. Ed.* 42, 3428–3430. doi: 10.1002/anie.200350912
- Guo, X., Zheng, S., Zhang, G., Xiao, X., Li, X., Xu, Y., et al. (2017). Nanostructured graphene-based materials for flexible energy storage. *Energy Storage Mater.* 9, 150–169. doi: 10.1016/j.ensm.2017.07.006
- Li, X., Xue, H., and Pang, H. (2017). Facile synthesis and shape evolution of well-defined phosphotungstic acid potassium nanocrystals as a highly efficient visible-light-driven photocatalyst. *Nanoscale* 9, 216–222. doi: 10.1039/C6NR07680G
- Lian, J., Duan, X., Ma, J., Peng, P., Kim, T., and Zheng, W. (2009). Hematite (α -Fe₂O₃) with various morphologies: ionic liquid-assisted synthesis, formation mechanism, and properties. *ACS Nano* 3, 3749–3761. doi: 10.1021/nn900941e
- Liang, H., Chen, W., Jiang, X., Xu, X., Xu, B., and Wang, Z. (2014). Synthesis of 2D hollow hematite microplatelets with tuneable porosity and their

AUTHOR CONTRIBUTIONS

HY and YulZ partly designed the experiments and wrote the manuscript. QH, JZ, YuaZ, XX, and YL assisted in the analysis and interpretation of the data. JT and FW proposed the project and revised the manuscript.

ACKNOWLEDGMENTS

The authors acknowledge financial support from the Taishan Outstanding Overseas Scholar Program of Shandong Province, China. The work was financially supported by the Natural Science Foundation of Shandong Province, China (Grant number: ZR2018JL021 and ZR2014EMQ011), the National Natural Science Foundation of China (Grant number: 51402160 and 51673103) and the Qingdao Postdoctoral Application Research Project. The work was also supported by the Opening Project of Key Laboratory of Microelectronic Devices & Integrated Technology, Institute of Microelectronics, Chinese Academy of Sciences, and the National Demonstration Center for Experimental Applied Physics Education (Qingdao University).

SUPPLEMENTARY MATERIAL

The Supplementary Material for this article can be found online at: <https://www.frontiersin.org/articles/10.3389/fchem.2019.00058/full#supplementary-material>

- comparative photocatalytic activities. *J. Mater. Chem. A* 2, 4340–4346. doi: 10.1039/c3ta14476c
- Liu, D. P., Li, G. D., Su, Y., and Chen, J. S. (2006). Highly luminescent ZnO nanocrystals stabilized by ionic-liquid components. *Angew. Chem.* 118, 7530–7533. doi: 10.1002/ange.200602429
- Lou, X. W., Wang, Y., Yuan, C., Lee, J. Y., and Archer, L. A. (2006). Template-free synthesis of SnO₂ hollow nanostructures with high lithium storage capacity. *Adv. Mater.* 18, 2325–2329. doi: 10.1002/adma.200600733
- Ma, J., Guo, X., Yan, Y., Xue, H., and Pang, H. (2018). FeO_x-based materials for electrochemical energy storage. *Adv. Sci.* 5:1700986. doi: 10.1002/advs.201700986
- Mao, D., Ding, S., Meng, L., Dai, Y., Sun, C., Yang, S., et al. (2017). One-pot microemulsion-mediated synthesis of Bi-rich Bi₄O₅Br₂ with controllable morphologies and excellent visible-light photocatalytic removal of pollutants. *Appl. Catal. B Environ.* 207, 153–165. doi: 10.1016/j.apcatb.2017.02.010
- Mele, A., Tran, C. D., and De Paoli Lacerda, S. H. (2003). The structure of a room-temperature ionic liquid with and without trace amounts of water: the role of C–H···O and C–H···F interactions in 1-n-Butyl-3-Methylimidazolium tetrafluoroborate. *Angew. Chem.* 115, 4500–4502. doi: 10.1002/ange.200351783
- Park, S. J., Kim, S., Lee, S., Khim, Z. G., Char, K., and Hyeon, T. (2000). Synthesis and magnetic studies of uniform iron nanorods and nanospheres. *J. Am. Chem. Soc.* 122, 8581–8582. doi: 10.1021/ja001628c
- Pawar, P., and Choi, D. (2015). Reduced graphene oxide composites with MWCNTs and single crystalline hematite nanorhombhedra for applications in water purification. *Int. J. Hydrogen Energy* 40, 767–778. doi: 10.1016/j.ijhydene.2014.08.084
- Ping, W., Zheng, Z., Cheng, X., Sui, L., Shan, G., Zhang, X. F., et al. (2017). Ionic liquid-assisted synthesis of α -Fe₂O₃ mesoporous nanorod arrays and their excellent trimethylamine gas-sensing properties for monitoring fish freshness. *J. Mater. Chem. A* 5, 19846–19856. doi: 10.1039/c7ta06392j
- Seddon, K. R. (2003). A taste of the future. *Nat. Mater.* 2:363. doi: 10.1038/nmat907

- Shikha, P., Randhawa, B., and Kang, T. (2015). Greener synthetic route for superparamagnetic and Luminescent α -Fe₂O₃ nanoparticles in binary mixtures of ionic liquid and ethylene glycol. *Rsc Adv.* 5, 51158–51168. doi: 10.1039/C5RA07218B
- Song, H. J., Jia, X. H., Qi, H., Yang, X. F., Tang, H., and Min, C. Y. (2012). Flexible morphology-controlled synthesis of monodisperse α -Fe₂O₃ hierarchical hollow microspheres and their gas-sensing properties. *J. Mater. Chem.* 22, 3508–3516. doi: 10.1039/c2jm13574d
- Sorescu, M., Brand, R. A., Mihaila-Tarabasanu, D., and Diamandescu, L. (1999). The crucial role of particle morphology in the magnetic properties of haematite. *J. Appl. Phys.* 85, 5546–5548. doi: 10.1063/1.369890
- Sun, Z., Yuan, H., Liu, Z., Han, B., and Zhang, X. (2010). A highly efficient chemical sensor material for H₂S: α -Fe₂O₃ nanotubes fabricated using carbon nanotube templates. *Adv. Mater.* 17, 2993–2997. doi: 10.1002/adma.200501562
- Tang, J., Zou, Z., and Ye, J. (2004). Effects of substituting Sr²⁺ and Ba²⁺ for Ca²⁺ on the structural properties and photocatalytic behaviors of CaIn₂O₄. *Chem. Mater.* 16, 1644–1649. doi: 10.1021/cm0353815
- Tong, G., Liu, Y., Wu, T., Ye, Y., and Tong, C. (2015). High-quality elliptical iron glycolate nanosheets: selective synthesis and chemical conversion into Fe_xO_y nanorings, porous nanosheets, and nanochains with enhanced visible-light photocatalytic activity. *Nanoscale* 7, 16493–16503. doi: 10.1039/C5NR03689E
- Wang, F. Y., Yang, Q. D., Xu, G., Lei, N. Y., Tsang, Y. K., Wong, N. B., et al. (2011). Highly active and enhanced photocatalytic silicon nanowire arrays. *Nanoscale* 3, 3269–3276. doi: 10.1039/c1nr10266d
- Wasserscheid, P., and Keim, W. (2000). Ionic liquids—new “solutions” for transition metal catalysis. *Cheminform* 39, 3772–3789. doi:10.1002/1521-3773
- Welton, T. (1999). Room-temperature ionic liquids: solvents for synthesis and catalysis. *Chem. Rev.* 99, 2071–2084. doi: 10.1021/cr980032t
- Wu, W., Hao, R., Liu, F., Su, X., and Hou, Y. (2013). Single-crystalline α -Fe₂O₃ nanostructures: controlled synthesis and high-index plane-enhanced photodegradation by visible light. *J. Mater. Chem A* 1, 6888–6894. doi: 10.1039/c3ta10886d
- Xia, J., Yin, S., Li, H., Xu, H., Xu, L., and Xu, Y. (2011a). Improved visible light photocatalytic activity of sphere-like BiOBr hollow and porous structures synthesized via a reactable ionic liquid. *Dalton Trans.* 40, 5249–5258. doi: 10.1039/c0dt01511c
- Xia, J., Yin, S., Li, H., Xu, H., Yan, Y., and Zhang, Q. (2011b). Self-assembly and enhanced photocatalytic properties of BiOI hollow microspheres via a reactable ionic liquid. *Langmuir* 27, 1200–1206. doi: 10.1021/la104054r
- Xiang, Q., Yu, J., and Wong, P. K. (2011). Quantitative characterization of hydroxyl radicals produced by various photocatalysts. *J. Colloid Inter. Sci.* 357, 163–167. doi: 10.1016/j.jcis.2011.01.093
- Xie, H., Li, Y., Jin, S., Han, J., and Zhao, X. (2010). Facile Fabrication of 3D-ordered macroporous nanocrystalline iron oxide films with highly efficient visible light induced photocatalytic Activity. *J. Phys. Chem. C* 114, 9706–9712. doi: 10.1021/jp102525y
- Xu, B., Huang, B., Cheng, H., Wang, Z., Qin, X., Zhang, X., et al. (2012). α -Fe₂O₃ hollow structures: formation of single crystalline thin shells. *Chem. Commun.* 48, 6529–6531. doi: 10.1039/c2cc33032f
- Xu, L., Xia, J., Wang, K., Wang, L., Li, H., Xu, H., et al. (2013). Ionic liquid assisted synthesis and photocatalytic properties of alpha-Fe₂O₃ hollow microspheres. *Dalton Trans.* 42, 6468–6477. doi: 10.1039/c3dt50137j
- Yang, S., Song, X., Zhang, P., Sun, J., and Gao, L. (2014). Self-assembled α -Fe₂O₃ mesocrystals/graphene nanohybrid for enhanced electrochemical capacitors. *Small* 10, 2270–2279. doi: 10.1002/smll.201303922
- Yu, J., Yu, X., Huang, B., Zhang, X., and Dai, Y. (2009). Hydrothermal synthesis and visible-light photocatalytic activity of novel cage-like ferric oxide hollow spheres. *Crystal Growth Des.* 9, 1474–1480. doi: 10.1021/cg800941d
- Yu, X., Yu, J., Cheng, B., and Huang, B. (2009). One-pot template-free synthesis of monodisperse Zinc sulfide hollow spheres and their photocatalytic properties. *Chem. A Eur. J.* 15, 6731–6739. doi: 10.1002/chem.200900204
- Zhang, D. E., Zhang, X. J., Ni, X. M., and Zheng, H. G. (2006). Preparation and characterization of α -FeOOH nanorods via an ethylenediamine-assisted route. *Mater. Lett.* 60, 1915–1917. doi: 10.1016/j.matlet.2005.12.053
- Zhao, G., Cheng, Y., Wu, Y., Xu, X., and Hao, X. (2018). New 2D carbon nitride organic materials synthesis with huge-application prospects in CN photocatalyst. *Small* 14: e1704138. doi: 10.1002/smll.201704138
- Zhao, G., Wang, T., Shao, Y., Wu, Y., Huang, B., and Hao, X. (2017). A novel mild phase-transition to prepare black phosphorus nanosheets with excellent energy applications. *Small* 13:201602243. doi: 10.1002/smll.201602243
- Zhou, X., Lan, J., Liu, G., Deng, K., Yang, Y., Nie, G., et al. (2011). Facet-mediated photodegradation of organic dye over Hematite architectures by visible light. *Angew. Chem. Int. Ed.* 51, 178–182. doi: 10.1002/anie.201105028
- Zhou, X., Xu, Q., Lei, W., Zhang, T., Qi, X., Liu, G., et al. (2014). Origin of tunable photocatalytic selectivity of well-defined α -Fe₂O₃ nanocrystals. *Small* 10, 674–679. doi: 10.1002/smll.201301870
- Zhu, L. P., Bing, N. C., Wang, L. L., Jin, H. Y., Liao, G. H., and Wang, L. J. (2012). Self-assembled 3D porous flowerlike α -Fe₂O₃ hierarchical nanostructures: synthesis, growth mechanism, and their application in photocatalysis. *Dalton Trans.* 41, 2959–2965. doi: 10.1039/c2dt11822j
- Zhu, L. P., Wang, L. L., Bing, N. C., Huang, C., Wang, L. J., and Liao, G. H. (2013). Porous fluorine-doped γ -Fe₂O₃ hollow spheres: synthesis, growth mechanism, and their application in photocatalysis. *ACS Appl. Mater. Inter.* 5, 12478–12487. doi: 10.1021/am403720r
- Zhu, L. P., Xiao, H.-M., Zhang, W. D., Yang, G., and Fu, S. Y. (2008). One-pot template-free synthesis of monodisperse and single-crystal magnetite hollow spheres by a simple solvothermal route. *Cryst. Growth Des.* 8, 957–963. doi: 10.1021/cg700861a

Conflict of Interest Statement: The authors declare that the research was conducted in the absence of any commercial or financial relationships that could be construed as a potential conflict of interest.

Copyright © 2019 Yin, Zhao, Hua, Zhang, Zhang, Xu, Long, Tang and Wang. This is an open-access article distributed under the terms of the Creative Commons Attribution License (CC BY). The use, distribution or reproduction in other forums is permitted, provided the original author(s) and the copyright owner(s) are credited and that the original publication in this journal is cited, in accordance with accepted academic practice. No use, distribution or reproduction is permitted which does not comply with these terms.